13th International Symposium on Particle Image Velocimetry – ISPIV 2019
Munich, Germany, July 22-24, 2019

Simultaneous measurements of flow velocity using Tomo-PIV and deformation of a flexible wing

Gwenaël Acher[1]*, Lionel Thomas[1], Benoit Tremblais[2], Guillaume Gomit[1], Ludovic Chatellier[1], Laurent David[1]

[1]CNRS – Université de Poitiers – ISAE-ENSMA, Institut PPRIME, UPR3346, Poitiers, France
[2]Université de Poitiers, Laboratoire XLIM, Axe ASALI/SRI, CNRS 7252, France

*gwenael.acher01@univ-poitiers.fr

Abstract

Fluid-structure interaction can lead to huge load fluctuations on mechanical structures and eventually cause irremediable damage. The simultaneous estimation of the displacement and/or the deformation of the structure, the flow topology around it and the induced stress is crucial to understand the physics of the interaction and anticipate the life-time of the device. In order to investigate this situation, we conducted an experiment around a flexible NACA0015 wing. The wing, of chord 80mm and span 146mm, has been molded in a polyurethane resin. It is placed in a hydrodynamic test section of size 230mm x 230mm at an angle of attack of 30°. The flow is set to 1.25 m/s, yielding a chord-based Reynolds number of 10^5. In this experimental configuration, synchronized measurements of the wing surface and of 3 dimensional – 3 components velocity fields have been recorded at a frequency of 2 kHz. Two high-speed cameras, placed under the test section, are set to observe the pressure side of the wing, on which a pattern has been painted to track the deformation. The surface reconstruction is performed using a parametric PIV/DIC method. Four additional high-speed cameras are set to record particle images of the velocity measurement volume and the scene is illuminated by two lasers to increase the global intensity of the particles and minimize the shadows due to the wing. The Tomo-PIV measurement is conducted using a home-made camera model based on the association of a polynomial model and a local discrete correction (Acher et al, 2018). The reconstruction is performed using a MART algorithm. Finally, FTEE algorithm (Jeon et al, 2014) has been used to benefit from the temporal resolution of the data. From the 3D3C velocity time series, the evolution of the pressure is deduced using the recently assessed algorithm presented in Gomit et al, 2018 (see Fig. 4). Two pressure taps inserted in the flow are used to initialize the pressure reconstruction and assess its reliability. Correlations between the flexible profile and the flow are observed and validated the coupling of the methods to measure the fluid structure interactions.

1 Introduction

Fluid-structure interaction can lead to huge load fluctuations on mechanical structures and eventually cause irremediable damage. The simultaneous estimation of the displacement and/or the deformation of the structure, the flow topology around it and the induced stress is crucial to understand the physics of the interaction and anticipate the life-time of the device. In hydrodynamics and aerodynamic applications, several configurations offer conditions where profiles are placed in a high-lift position with large angle of attack (for examples foil, wind and water turbines, boat appendices. In such situations, the flow is largely detached and the vortex shedding generates high temporal variations of the loads and deformation of the structure.

In the context of flow measurements, the 3 components of the velocity can now be obtained using Tomo-PIV and 3D PTV and it allows the evaluation of the pressure field in thick measurement volumes. It is also possible to measure the displacement and the deformation of the wing, synchronously with the flow measurements.

In this paper, measurements of the 3D deformation of a NACA0015 flexible wing profile and the 3D flow around it are applied at a Reynold number of 10^5. Wing time-deformation, volumetric instantaneous velocity fields, and pressure fields are measured and correlated to show mutual influence between the flow and the wing. This combination of different techniques is a promising way of studying the fluid-structure interactions.

2 Experimental setups

Devices and flow

A wing profile of 146 mm span is placed at 30° angle of attack in the test section of a hydrodynamic tunnel. The NACA0015-type wing profile, based on a 80 mm chord, is built of a 140 mm long straight section and its tip is formed by the rotation of the profile around the chord, adding 6mm of wingspan, at the position of maximum thickness. A rectangular base, embedded in the wall, is used to fix the profile on a 6-component ATI Nano17 balance (IP68). A schematic of the profile-balance-window mounting is shown in **Figure 1**. The wing is molded in polyurethane to provide flexibility. Finally, the flow velocity is set at 1.25 m/s, setting the Reynolds number based on the chord at 10^5.

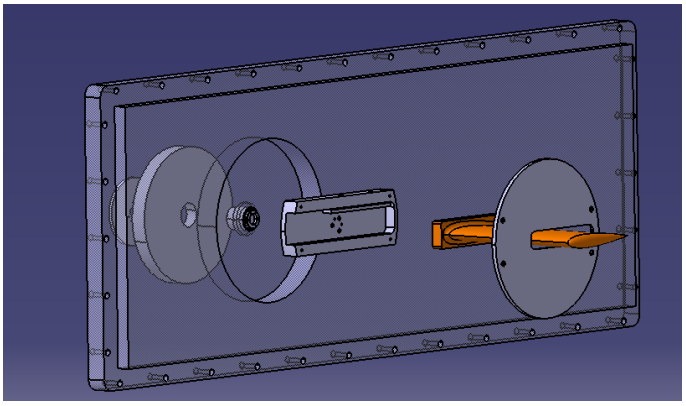

Figure 1: Schematic of the wing profile and its support in the wall.

In this investigation, coupled measurements of velocity by Tomo-PIV, surface tracking by the method HNC (Height Normal Curvature) and pressure are carried out in this flow configuration. The equipment is shown in **Figure 2**. The load measurement, initially planned in association with the three previous metrology techniques, could not be performed because of a dysfunction of the balance. It was finally carried out, *a posteriori*, with coupled pressure measurements.

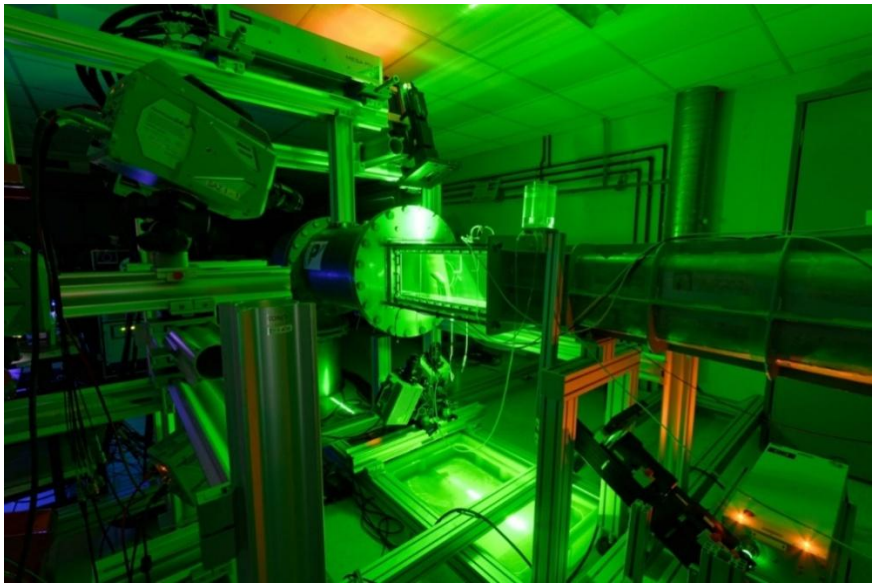

Figure 2: Experimental device of the test section with the two lasers and the six cameras.

Tomo-PIV measurements

Tomo-PIV velocity measurements are obtained from five key steps. The first step is to calibrate the optical system consisting of four high-speed cameras (2 Photron Fastcam APX-RS + 2 Photron Fastcam SA-Z) observing the measurement area. The cameras are arranged according to a pyramidal base but a camera is moved in central position (**Table 1**), in order to better resolve the wake. This calibration step enables to establish geometric relations between the particle images and the measured fluid volume. The calibration of the system is carried out using a calibration chart moved according to the depth. In order to correct the distortions related to the presence of thick windows, the model used is a hybrid polynomial-discrete model developed within the institute (Acher et al., 2018). It combines a discrete local correction with an analytical model, thus improving the accuracy of the triangulation model.

	Camera 1	Camera 2	Camera 3	Camera 4
rx	-18	18	-18	0
ry	-16	16	16	0

Table 1: Camera location in the Tomo-PIV experiment

In order to visualize the flow, small polyamide particles (Vestosint) with a diameter of 50 µm were seeded into the fluid. Then the measuring volume is illuminated with two high-speed lasers

(Continuum TerraPIV and MesaPIV) to ensure a sufficient light intensity and limit the shadow effects related to the presence of the profile in the measurement field. The particle images are recorded simultaneously by the four cameras of the system at a frequency of 2kHz, and then filtered to limit the impact of measurement noise on subsequent steps.

In order to correct a possible displacement of the optical system between the calibration step and the measurement and to refine the different models, a misalignment correction step is performed. This operation, always necessary in practice, makes possible to relate the four camera models in order to increase the accuracy of the particle localization in the volume. The discrete correction of the hybrid model, used for this experiment, is initialized during this step. The series of particle volumes, separated by a time step Δt, is then reconstructed from the images of the particles, recorded at each measurement step, and the projection functions. In this study, a discrete reconstruction technique (voxel approach) was used. The chosen algorithm is MART (Multiplicative Algebraic Reconstruction Technique) in which the weighting functions are computed taking into account the intersection between a spherical modeled voxel and the line of sight corresponding to the investigated pixel (Thomas et al. 2014). Finally, the particle displacement field is determined by a local inter-correlation calculation between multiple consecutive instants. The correlation in this study is carried out using the FTEE algorithm (Jeon et al, 2014) which enables to take advantage of the temporal resolution of the data series. The algorithm calculates a polynomial trajectory of a small group of particles over a series of N frames, providing an estimate of the velocity with increased accuracy and a measure of the Lagrangian acceleration for the central instant. The correlation is completed with a series of 9 images, interrogation volumes of 32x32x32 voxels size and 75% of overlap, providing a spatial resolution of 0.65 vector / mm.

The velocity measurement was carried out around the profile in three sections of the flow centered on the z = 70 mm, z = 105 mm and z = 140 mm planes, respectively corresponding to 0.5 wingspan, 0.75 wingspan and wingtip (here the positions are based on the span of the straight section, see **Figure 3**). The measurement volumes are about 180 mm in the x and y directions and 16 mm and 22 mm in thickness, two thicknesses having been made for each case. An instantaneous velocity field, extracted from the series carried out at mid-span, is presented in **Figure 4**.

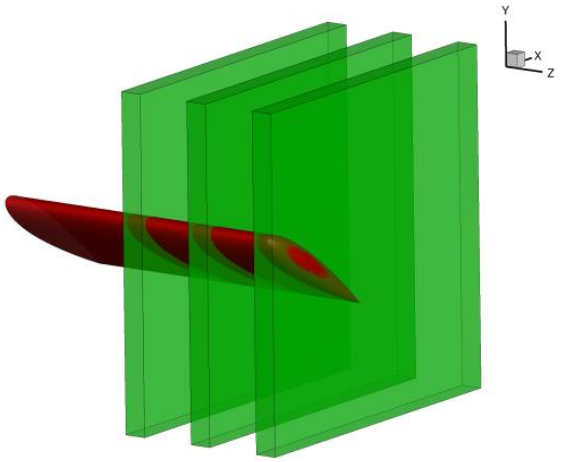

Figure 3: Sections of Tomo-PIV measurements

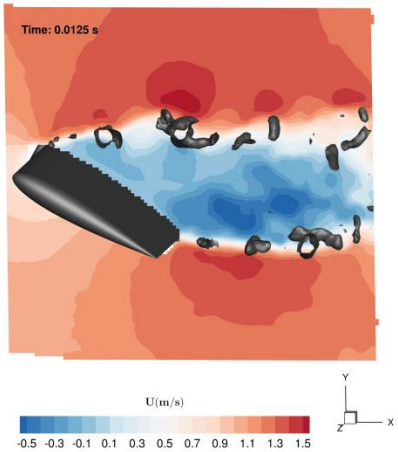

Figure 4: Streamwise velocity component and iso contour of Q criterion obtained by Tomo-PIV.

DIC method for displacement and deformation measurement

The surface measurement used in this study, based on a DIC method, is described by Chatellier et al. (2013). The technique is based on maximizing the correspondence of two back-projected images on the estimated solid surface. In order to follow the deformation of the wing profile in the test section, a speckle pattern is painted on its pressure side and two high speed cameras (Photron Fastcam SA1.1) are placed under the water tunnel in observation of this one. The position of the cameras is visible in the photograph of the experiment (**Figure 2**) and the recorded images are shown in **Figure 5.**

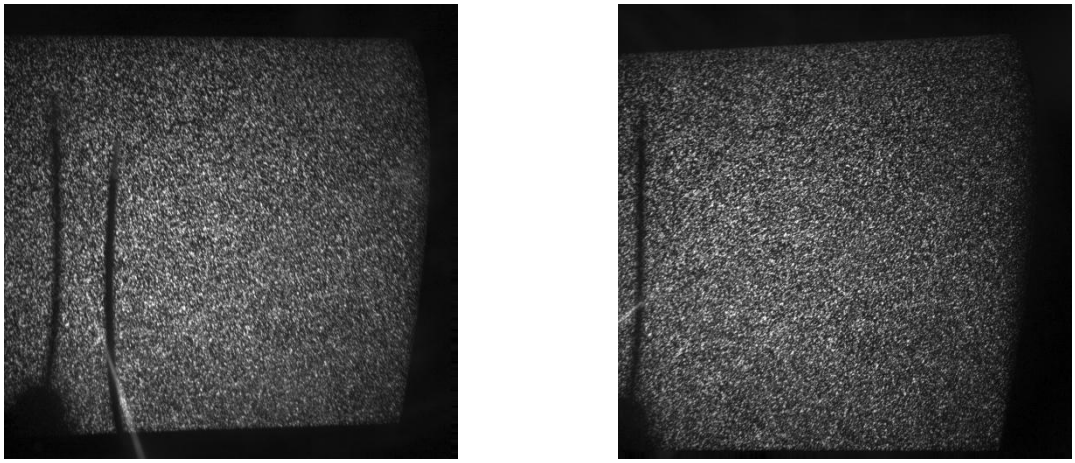

Figure 5: Left and right images used for the wing surface estimation.

The image processing is done in the following way: The domain is described in a Cartesian coordinate system where the plane y = 0 corresponds to the average plane of the wing profile. A mesh (x_0,0, z_0), whose nodes correspond to the 2D points where the surface is estimated, is created and refined in areas of steep slope (**Figure 6**). The mesh is narrowed at the leading edge (upper part of the mesh), the trailing edge (lower part) and the wingtip (right part of the mesh). Each point of this mesh is the subject of a local estimation of its altitude y_0 and the local slopes dy/dx and dy/dz according to the procedure presented below.

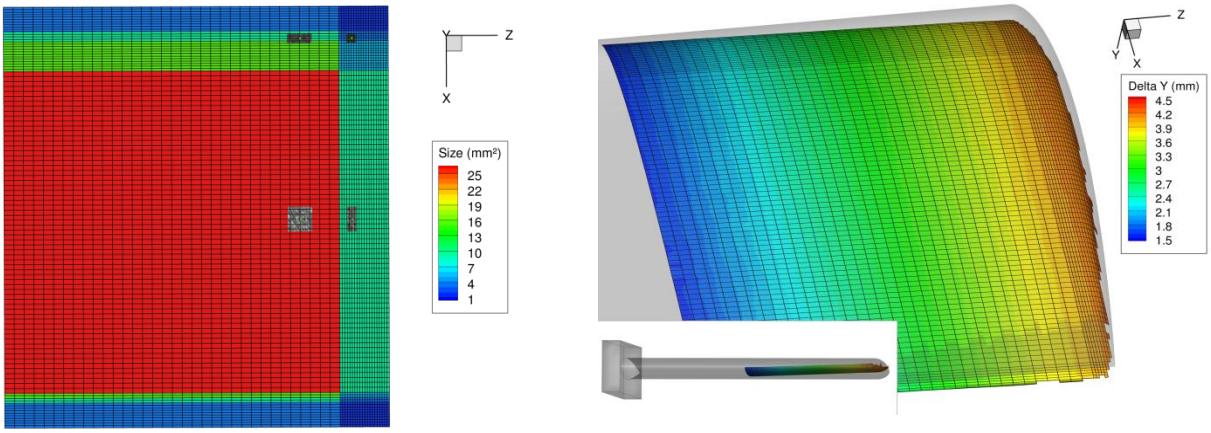

(a) Mesh of the reconstructed surface

(b) Reconstructed surface for the flexible wing and displacement compared to its position at rest.

Figure 6: Mesh and reconstructed surface by the HNC method

At first, a local mesh around the point (x_0, z_0) is generated. The size and number of mesh points are adjusted to take into account the direction of local gradients. The mesh size should approximate the size of the one-pixel back-projection of the image on the surface. Then, the area (x, y, z), centered around (x_0, z_0), is parameterized by an altitude y_0 and local slopes as follows:

$$y = y_0 + \frac{\partial y}{\partial x}(x - x_0) + \frac{\partial y}{\partial z}(z - z_0)$$

The left and right images are back-projected on this surface (nodes of the local mesh) and compared by correlation to determine their similarity. The parameters of the surface (y_0, dy/dx, dy/dz) are optimized with the target of maximizing the correlation coefficient.

The reconstruction of the surface of the wing profile is illustrated in **Figure 6** (b), where the surface of the flexible wing is represented at a given time of the time series and colored by the local changes of altitude with respect to its position at rest (modeled by the transparent gray volume).

Pressure evaluation

The pressure calculation strategy adopted here is based on the work of Jeon et al. (2018) and relies on integrating the pressure gradient of the Navier-Stokes equations. The different terms composing the pressure gradient are calculated from the PIV measurements. An iterative pseudo-Lagrangian approach (ILAG, Lynch and Scarano 2014) is applied in order to obtain material acceleration from the velocity fields based on a second order polynomial trajectory. The pressure field is then obtained by minimizing a functional in a least-square sense, built on the difference between the pressure gradient based on the PIV measurements and the estimated pressure gradient, which is equivalent to solving a Poisson equation.

Prior to the integration step, as explained in Jeon et al. (2017), the integration domain is generally divided in sub-domains in accordance with the local reliability, based on the local variation of the pressure gradient. The sequential pressure reconstruction is initiated from the outer domain, where higher measurement accuracy is expected, hence where a reliable pressure reference can be taken. This reference pressure is calculated based on Bernoulli's principle as :

$$P(\mathbf{x}) = \frac{1}{2}\rho(U_\infty^2 - U(\mathbf{x})^2)$$

The pressure field in the other sub-domains is then computed by imposing Dirichlet boundary conditions from the previously computed domain. In the case of a wing, these subdomains can be defined as the outer region, wake, near-body, near-edge and masked.

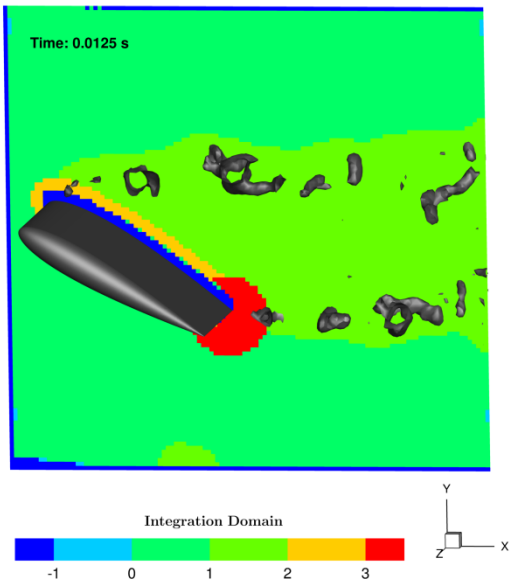

Figure 7: Integration domains definition for pressure computation

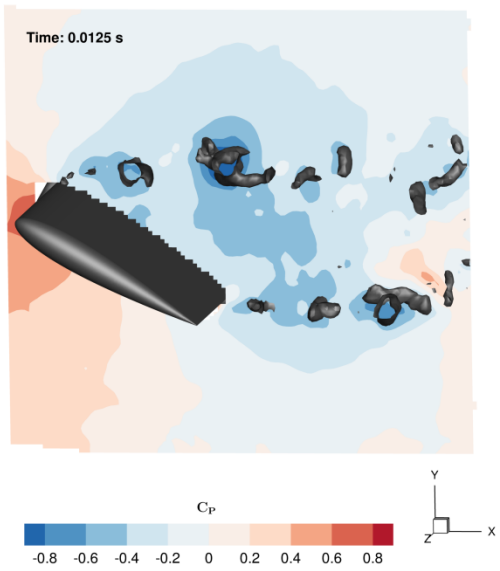

Figure 8: 3D Pressure field computed from the experimental velocity data

3 Results and comparison

Flow

The streamwise velocity and pressure coefficient are plotted for the three measurement volumes in **Figure 9**, **Figure 10** and **Figure 11**, respectively for section 70 mm, 105 mm and the wingtip. As expected, it is clearly visible that the wake reduces in size along the wingspan. The streamwise overspeed also tends to decrease along the wingspan due to the wake thickness reduction and the blockage effect attenuation.

The coherent structures, in the shear layers close to the wing are mainly two-dimensional and rapidly the three-dimensionality, expected at such high Reynolds and high angle of attack, appears. Close to the wing tip, long streamwise coherent structures can be observed.

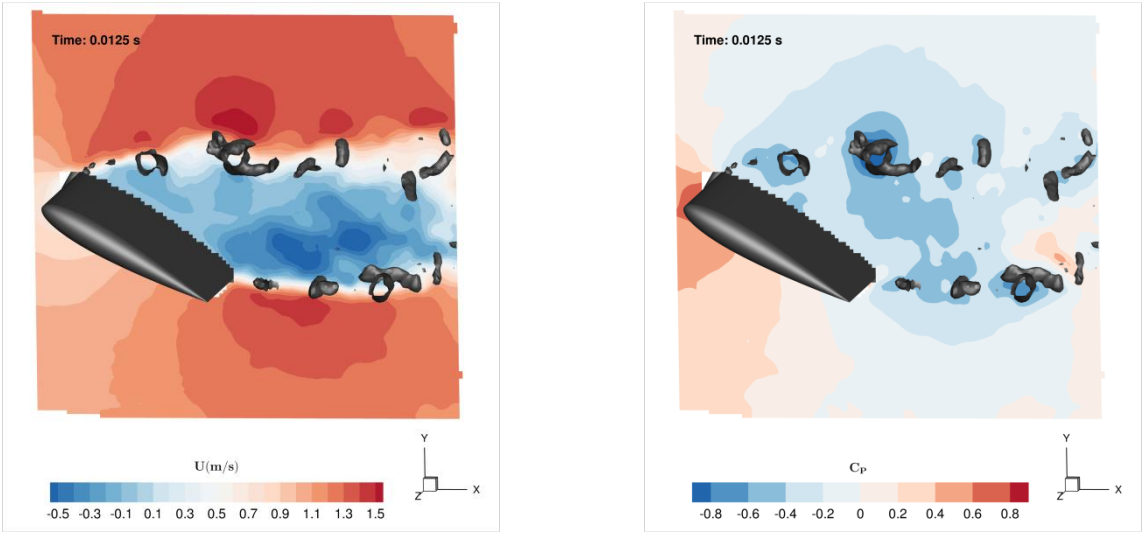

Figure 9: Streamwise velocity (left) and Pressure coefficient (right) with Q criterion iso-surfaces in plane 70 mm

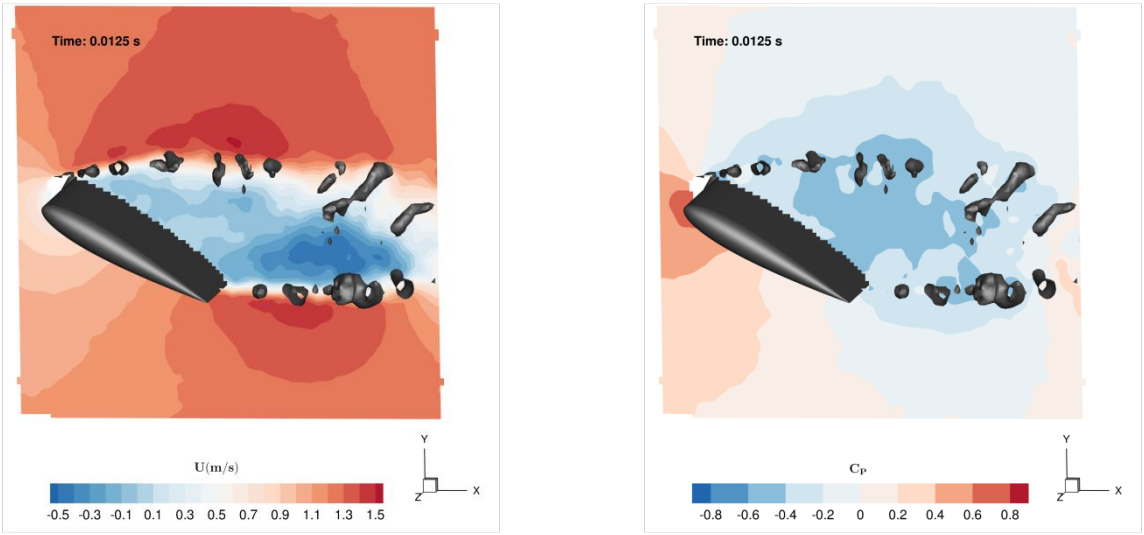

Figure 10: Streamwise velocity (left) and Pressure coefficient (right) with Q criterion iso-surfaces in plane 105 mm

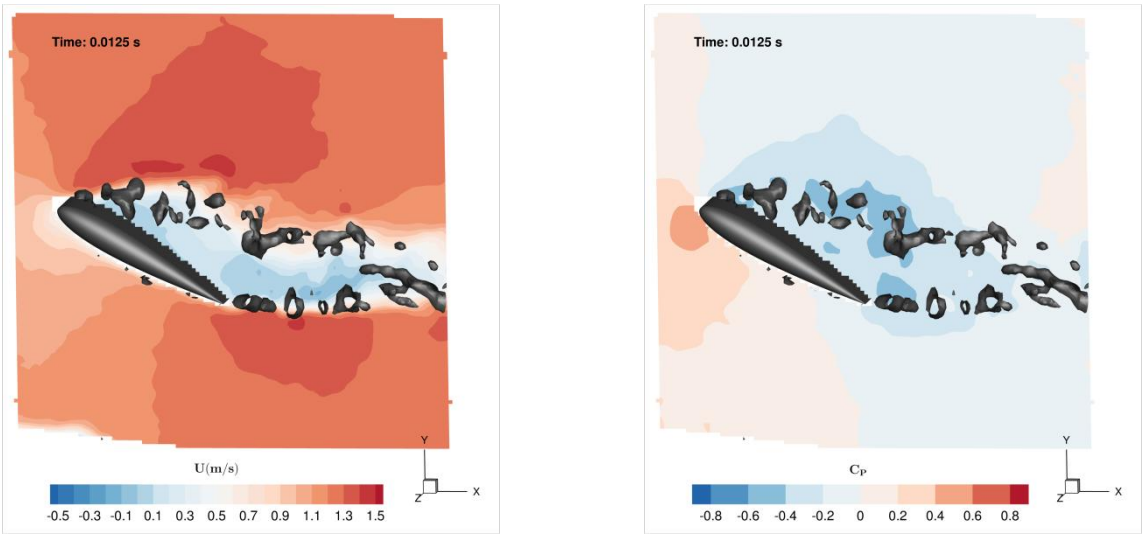

Figure 11: Streamwise velocity (left) and Pressure coefficient (right) with Q criterion iso-surfaces in plane 140 mm

Deformation

The temporal evolution of the surface can be extracted from the reconstructed surfaces. The response of the wing to the fluid loads mainly consists in a beam-like bending due to the time-average values of the pressure distribution. The resulting average displacement is of the order of 3mm at the tip of the wing.

The unsteadiness of the wing deformation is evidenced on **Figure 12**. The time-history of a chosen point on the wing-tip indicates that the free-end of the wing is subject to oscillations of the order of 300 µm in amplitude (10% of the average displacement).

Superimposed on the time history of the surface height is plotted the vertical velocity extracted at a point in the shear layer, 1.5 chord downstream from the leading edge (shifted in time). It seems that a correlation between the two signals exists.

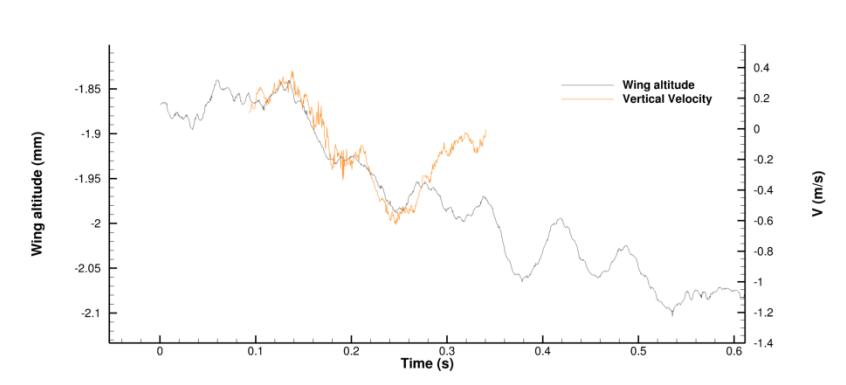

Figure 12: Altitude variation of a surface point around the wingtip at quarter of chord

4 Conclusion and Perspectives

Synchronized measurements of the wing deformation and three-dimensional velocity around a wing profile, using Tomo-PIV, have been successfully performed in a high Reynolds, high angle of attack configuration. Although it appears there is a link between the flow characteristics and the wing deformation, the velocity time series are, at this point, too short to draw sound conclusions. The remaining instants of the velocity time series are currently under computation. Once they are fully computed, the correlation between the flow features and the structure movements will be performed and analyzed.

Acknowledgement

The current work has been conducted as part of the Homer project, Holistic Optical Metrology for Aero-Elastic Research funded by the European Commission, program H2020, Grant No. No. 769237 and as part of the EVAPOR Astrid project, funded by the Agence Nationale de la Recherche and the DGA, Grant No. NR-16-ASTR-0005-01. The grant of Gwenaël Acher's PhD thesis is supported by the Direction Générale de L'Armement.

References

Acher G, Thomas L, Tremblais B, and David L (2018) A new camera model combining a pinhole model and a discrete correction to overcome refractive index variation challenges. *Lisbon 2018, Portugal, July 16 – 19*

Chatellier L, Jarny S, Gibouin F, and David L (2013) A parametric PIV/DIC method for the measurement of free surface flows. *Experiments in fluids* 54:1488

Gomit G, Acher G, Chatellier L, and David L (2018) Uncertainty analysis of an optical method for pressure estimation in fluid flows. *Measurement Science and Technology* 29:024004

Jeon YJ, Chatellier L, and David L (2014) Fluid trajectory evaluation based on an ensemble-averaged cross-correlation in time-resolved PIV. *Experiments in Fluids* 55:1766

Jeon YJ, Gomit G, Earl T, Chatellier L and David L (2018) Sequential least-square reconstruction of instantaneous pressure field around a body from TR-PIV. *Experiments in Fluids* 59:27

Lynch KP and Scarano F (2014) Material acceleration estimation by four-pulse tomo-PIV. *Measurement Science and Technology* 25:084005

Thomas L, Tremblais B, and David L (2014) Optimization of the volume reconstruction for classical tomo-piv algorithms (mart, bimart and smart): synthetic and experimental studies. *Measurement Science and Technology* 25:035303